Title

Molecular Interactions in the Voltage Sensor Controlling Gating Properties of CaV Calcium Channels

Journal

Structure, 24(2)

ISSN

1359-0278

Authors

Tuluc, Petronel
Yarov-Yarovoy, Vladimir
Benedetti, Bruno
et al.

Publication Date

2016-02-01

DOI

10.1016/j.str.2015.11.011

Peer reviewed

Research Article

Structure

Molecular Interactions in the Voltage Sensor Controlling Gating Properties of Ca_V Calcium Channels

Highlights

- S3-S4 linker lengths in Ca_V channels control their voltage sensitivity
- Rosetta modeling predicts that the S3-S4 linker determines the charge transfer
- Mutagenesis has identified a new counter charge in S3 of Ca_V critical for gating

Authors

Petronel Tuluc,
Vladimir Yarov-Yarovoy,
Bruno Benedetti, Bernhard E. Flucher

Correspondence

petronel.tuluc@uibk.ac.at (P.T.),
bernhard.e.flucher@i-med.ac.at (B.E.F.)

In Brief

Voltage-gated calcium channels (Ca_V) translate membrane depolarization into calcium influx that regulates muscle contraction, hormone secretion, or synaptic transmission. Using computational structural modeling, site-directed mutagenesis, and electrophysiology, Tuluc et al. identified the mechanism responsible for the different voltage sensitivities of two $Ca_V1.1$ calcium channel splice variants.

Tuluc et al., 2016, Structure *24*, 1–11
February 2, 2016
http://dx.doi.org/10.1016/j.str.2015.11.011

CellPress

Please cite this article in press as: Tuluc et al., Molecular Interactions in the Voltage Sensor Controlling Gating Properties of Ca_V Calcium Channels, Structure (2016), http://dx.doi.org/10.1016/j.str.2015.11.011

Structure
Research Article

Molecular Interactions in the Voltage Sensor Controlling Gating Properties of Ca_V Calcium Channels

Petronel Tuluc,[1,2,4,*] Vladimir Yarov-Yarovoy,[3,4] Bruno Benedetti,[1] and Bernhard E. Flucher[1,*]
[1]Department of Physiology and Medical Physics, Medical University Innsbruck, Fritz-Pregl-Strasse 3, A-6020 Innsbruck, Austria
[2]Department of Pharmacology and Toxicology, Institute of Pharmacy, University of Innsbruck, Innrain 80-82, A-6020 Innsbruck, Austria
[3]Department of Physiology and Membrane Biology, UC Davis, Davis, CA 95616, USA
[4]Co-first author
*Correspondence: petronel.tuluc@uibk.ac.at (P.T.), bernhard.e.flucher@i-med.ac.at (B.E.F.)
http://dx.doi.org/10.1016/j.str.2015.11.011

SUMMARY

Voltage-gated calcium channels (Ca_V) regulate numerous vital functions in nerve and muscle cells. To fulfill their diverse functions, the multiple members of the Ca_V channel family are activated over a wide range of voltages. Voltage sensing in potassium and sodium channels involves the sequential transition of positively charged amino acids across a ring of residues comprising the charge transfer center. In Ca_V channels, the precise molecular mechanism underlying voltage sensing remains elusive. Here we combined Rosetta structural modeling with site-directed mutagenesis to identify the molecular mechanism responsible for the specific gating properties of two $Ca_V1.1$ splice variants. Our data reveal previously unnoticed interactions of S4 arginines with an aspartate (D1196) outside the charge transfer center of the fourth voltage-sensing domain that are regulated by alternative splicing of the S3-S4 linker. These interactions facilitate the final transition into the activated state and critically determine the voltage sensitivity and current amplitude of these Ca_V channels.

INTRODUCTION

Voltage-gated calcium (Ca_V) channels contribute to the excitability of nerve and muscle cells and are the exclusive molecular agents to convert membrane depolarization into calcium-mediated cellular functions like muscle contraction, secretion of neurotransmitters and hormones, and gene regulation (Catterall, 2011). In mammals, Ca_V channels constitute a family of ten genes each with multiple splice variants. These give rise to functionally diverse channels, which activate at greatly different membrane potentials, precisely tuned to the specific requirements of the cell function they regulate (Lipscombe et al., 2013). Whereas voltage sensing in voltage-gated potassium (K_V) and sodium (Na_V) channels is well studied, the molecular details of the voltage-sensing mechanism in Ca_V channels are still elusive.

Ca_V α_1 subunits are polypeptides of more than 1,800 amino acids folded into four homologous repeats (I–IV) with six transmembrane segments each (S1–S6). Segments S1–S4 of each repeat form the voltage-sensing domains (VSD), while segments S5 and S6 with the connecting P loop form the channel pore and selectivity filter (Figure 1A). The S4 transmembrane segments of Ca_V channels contain four to five positively charged amino acids (arginines or lysines) spaced at three-amino acid intervals that serve as the actual voltage sensors of the voltage-dependent gating mechanism (Bezanilla, 2000; Bezanilla et al., 1991; Catterall, 2010; Kontis and Goldin, 1997; Noceti et al., 1996; Papazian et al., 1991; Seoh et al., 1996). In response to membrane depolarization, the S4 segments translocate toward the extracellular side of the membrane, inducing a conformational change of the S5 and S6 segments that leads to the opening of the channel pore (Ahern and Horn, 2004; Catterall and Yarov-Yarovoy, 2010; Yarov-Yarovoy et al., 2006a). To facilitate the movement of the S4 segments through the dielectric interior of the plasma membrane, the S1–S3 helices of the VSD contain several negatively charged and polar residues that stabilize the positive charges of S4 (Bezanilla, 2000; Catterall, 2010; Lacroix et al., 2014; Pless et al., 2014). In K_V and Na_V channels, three highly conserved residues have been identified as a "gating charge transfer center" (CTC) including a phenylalanine in S2 and negatively charged residues in S2 and S3 (Payandeh et al., 2011, 2012; Tao et al., 2010). These residues form transient hydrogen bond (H-bond) pairs with the positive gating charges of S4 as they sequentially pass through the CTC (Cheng et al., 2013; Lin et al., 2011; Tao et al., 2010; Yarov-Yarovoy et al., 2012). In the VSD of Ca_V channels, corresponding residues are also highly conserved.

Previously we described a splice variant of $Ca_V1.1$ ($Ca_V1.1e$, α_{1S}-ΔE29) lacking exon 29, which encodes 19 amino acids in the extracellular linker connecting transmembrane segments S3 and S4 in the fourth VSD (Figure 1A) (Flucher and Tuluc, 2011; Tuluc and Flucher, 2011; Tuluc et al., 2009). The shorter IVS3-S4 linker of $Ca_V1.1e$ confers the channel a ~30-mV left shift in voltage sensitivity and a ~6-fold increased current amplitude compared with the long IVS3-S4 linker of $Ca_V1.1a$. This indicates that, in the full-length $Ca_V1.1a$ channel, the VSD of the fourth repeat is limiting for voltage sensitivity and current amplitude. Since similar alternative splicing of the IVS3-S4 linker is found in most *CACNA1* genes, regulation of gating properties by the

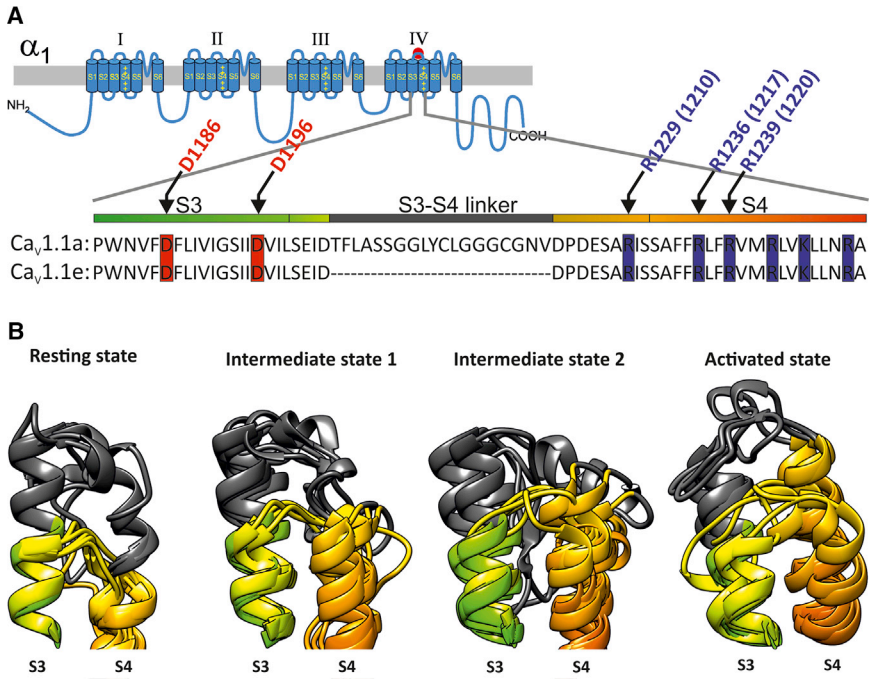

Figure 1. Structural Modeling of the IVS3-S4 Loop in Different Conformational States Depicts a Higher Variability of $Ca_V1.1a$ Loop Compared with $Ca_V1.1e$

(A) Transmembrane topology of the α_1 subunit of the voltage-gated calcium channels consisting of four repeats with six transmembrane domains each. The red mark indicates the position of exon 29 in the extracellular loop connecting IVS3 and IVS4. The sequence alignment of IVS3, the IVS3-S4 extracellular loop, and IVS4 of the two $Ca_V1.1$ splice variants shows the position of the 19 amino acids encoded by exon 29 in the IVS3-S4 linker, the positions of the positive charges in IVS4 (blue) and potential negative counter charges in IVS3 (red). Note that the colors of the bar above the sequences match the ribbon models below (green, S3; gray, exon 29; orange, S4).

(B) Predicted conformations of both $Ca_V1.1a$ and $Ca_V1.1e$ IVS3-S4 loops in the resting state, intermediate states 1 and 2, and in the activated state. Gray highlights the extra 19 amino acids encoded by exon 29 present in the $Ca_V1.1a$ loop, while the short IVS3-S4 linker of $Ca_V1.1e$ is depicted in yellow. Note the substantial conformational changes of the $Ca_V1.1a$ IVS3-S4 loop during gating and between different clusters, but less for the $Ca_V1.1e$ IVS3-S4 loop. The images were generated using UCSF Chimera (Pettersen et al., 2004).

fourth VSD may be a general principle for the specific gating properties of Ca_V channels (Liao et al., 2005; Lipscombe et al., 2013).

Here we addressed the molecular mechanism by which differences in the IVS3-S4 linker control the voltage sensitivity and amplitude of the two functionally distinct $Ca_V1.1$ channel variants. Using the Rosetta-Membrane method (Yarov-Yarovoy et al., 2006a, 2006b, 2012), we predicted the structure of the S3-S4 loop and the gating transitions of the VSD in both $Ca_V1.1$ channel splice variants. The structural models indicate that, in $Ca_V1.1e$ but not in $Ca_V1.1a$, H-bonds are forming between D1196 (in IVS3) and R1 and R2 (in IVS4) during the final steps of the gating charge movement. Using site-directed mutagenesis, we confirmed that the D1196 negatively charged residue in IVS3 is critical for electrostatic compensation of S4 charges and therefore determines the channel voltage sensitivity. Inclusion of exon 29 in the IVS3-S4 linker or mutation of D1196 (in IVS3) weakens the H-bonds between S4 charges and D1196 thus inducing a rightward shift in the voltage sensitivity of $Ca_V1.1a$.

RESULTS

Structure Prediction of the Fourth VSD of $Ca_v1.1a$ and $Ca_v1.1e$ Channels

We generated structural models of the fourth VSD of $Ca_v1.1a$ and $Ca_v1.1e$ channels using the Rosetta-Membrane method to reveal the structural basis for the critical role of the IVS3-S4 linker in determining voltage sensitivity (Yarov-Yarovoy et al., 2006a, 2006b, 2012). In order to identify the critical gating transition affected by the IVS3-S4 linker lengths (with and without the exon 29 sequence), the position of the S4 segment in relation to the CTC was modeled in four different conformational states (resting, intermediate 1, intermediate 2, and activated) as described in the Experimental Procedures. After several steps of selection and refinement, the top 10% of the best scoring models of the VSD in each conformational state are clustered and chosen for further visual evaluation and analysis. Although we observed a certain degree of variability between the different top clusters, a common feature of all top cluster models of the long $Ca_V1.1a$ IVS3-S4 linker is that the exon 29 sequence further extends the alpha helix of IVS3 toward the extracellular side of the membrane (Figure 1B). In the resting and intermediate states 1 and 2, all top cluster models show the $Ca_V1.1a$ IVS3-S4 linker orientated toward the outer vestibule of the VSD, while in the activated state, the IVS3-S4 linker bends away from the vestibule. Theoretically, these structural differences between the S3-S4 loops of the two $Ca_V1.1$ splice variants could alone alter the position or restrict the movement of the VSD transmembrane segments and thus explain the differences in voltage sensitivity.

Relaxed Homology Structure Models Reveal Differences in Packing and H-Bond Formation of the $Ca_V1.1a$ and $Ca_V1.1e$ VSDs

In order to test if the structurally divergent IVS3-S4 linkers differentially affect the VSD structure, and thus the voltage sensitivity of the two $Ca_V1.1$ splice variants, we relaxed the backbone and side-chain atoms in our homology models of the fourth VSD with the short and long IVS3-S4 linker. After full-atom relax, the VSD models of both splice variants in each conformational state reach similar low energy levels, indicating that the IVS3-S4 linker does not restrict the S4 movement. Previously it has been demonstrated that gating of

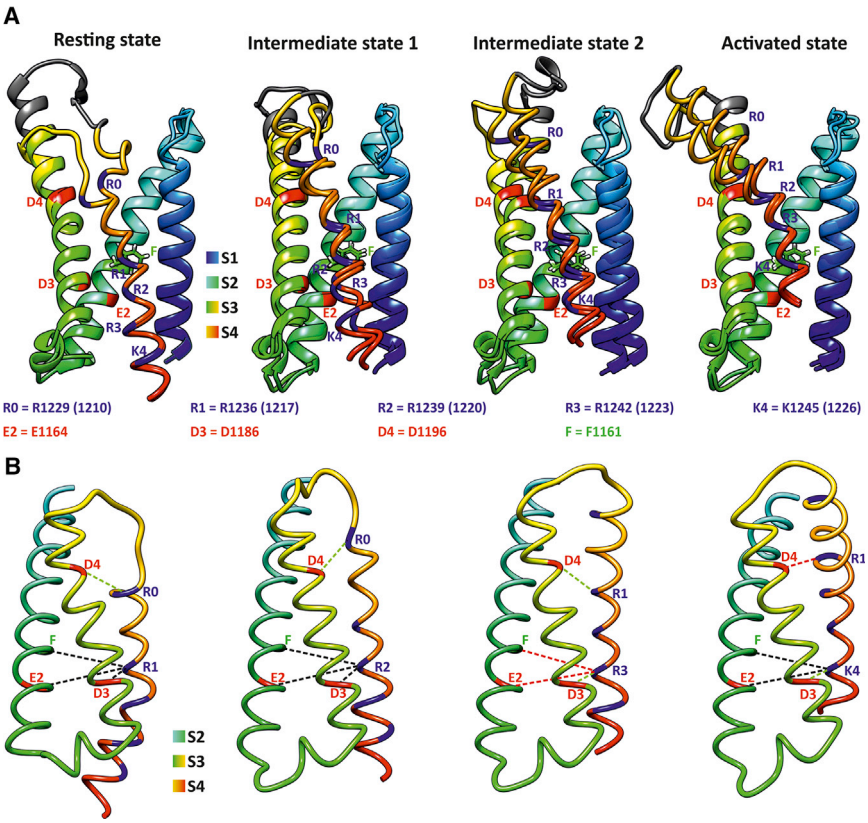

Figure 2. Homology Rosetta Modeling of the $Ca_V1.1$ Splice Variants Fourth Repeat VSD Gating States

(A) Superimposed structures of $Ca_V1.1a$ and $Ca_V1.1e$ VSD at the resting state, intermediate states 1 and 2, and the activated state. S1–S3 are shown as ribbons while the S4 transmembrane domain is shown as licorice to facilitate observation of similarities and differences in the structures of $Ca_V1.1a$ and $Ca_V1.1e$. The phenylalanine "cap" is shown to indicate the position of the CTC. In the fourth VSD of $Ca_V1.1$, the CTC comprises a phenylalanine (F1161 = F) and a glutamate (E1164 = E2) in IVS2, and an aspartate (D1186 = D3) in IVS3. S4 positively charged arginines are highlighted in blue, while the negatively charged amino acids that could participate to the charge transfer are highlighted in red. The extra 19 amino acids encoded by exon 29 in $Ca_V1.1a$ are shown in gray.

(B) Distance measurements between the C^{α} atoms of IVS4-charged amino acids and the C^{α} atoms of F and E2 in IVS2, D3, and D4 (D1196) in IVS3. Only S2, S3, and S4 of $Ca_V1.1e$ are shown for clarity. Black dotted lines indicate that the distances are the same in $Ca_V1.1a$ and $Ca_V1.1e$ in a given state, green dotted lines indicate that the distance is larger in $Ca_V1.1e$ compared with $Ca_V1.1a$, while red dotted lines indicate that the distance is larger in $Ca_V1.1a$ compared with $Ca_V1.1e$ by at least 0.2 Å. Distances in the CTC differ in the intermediate state 2 and the activated state, whereas S3-S4 distances near the IVS3-S4 linker (as indicated by D4 to the closest arginine in S4 substantially differ in all states. Distances are measured using UCSF Chimera (Pettersen et al., 2004) and the values are presented in Table 1.

Shaker potassium channels requires the formation of salt bridges of the basic residues in S4 with several acidic residues in the transmembrane helices S1, S2, and S3. These residues are E1 (E283) and E2 (E293) in the transmembrane helix S2 and D3 (D316) in the transmembrane helix S3 (Ma et al., 2006; Pless et al., 2011; Seoh et al., 1996). In Ca_V channels, the key residues of the CTC (E2, F, and D3) are conserved with those previously described for K_V (Lacroix et al., 2014; Tao et al., 2010) and Na_V channels (DeCaen et al., 2008, 2009, 2011; Yarov-Yarovoy et al., 2012), but in the fourth VSD of $Ca_V1.1$ channels, the counter charge corresponding to Shaker E1 is missing. The sequential movement of the positively charged S4 residues past the negative counter charges (E2, D3) and over the hydrophobic cap (phenylalanine) of the CTC is considered essential for the voltage-sensing process (Lacroix et al., 2014; Tao et al., 2010; Yarov-Yarovoy et al., 2012). The superimposed structural models (Figure 2A) show that the different size IVS3-S4 linkers do not dramatically change the general position of the IVS4 helix relative to the other helices of the VSD. However, especially in the intermediate state 2 and in the activated state, the outer parts of the IVS3 and IVS4 helices are displaced in $Ca_V1.1a$ relative to $Ca_V1.1e$, indicative of the impact of the IVS3-S4 linker on the structure of the VSD. Two morphs were generated to facilitate the visualization of the structural changes in the fourth VSD of $Ca_V1.1$ variants during gating (see Movies S1 and S2 related to Figure 2).

To quantitatively describe differences in the structure of the CTC of $Ca_V1.1a$ and $Ca_V1.1e$, we measured the distances between the C^{α} atoms of the positive charges in IVS4 relative to F, E2, and D3 in all four conformational states (Figure 2B and Table 1). In the resting and intermediate state 1, the intramolecular distances within the CTC were similar for both $Ca_V1.1$ splice variants. In intermediate state 2, the distances from F and E2 to R3 were shorter, while D3 to R3 was longer in $Ca_V1.1e$ compared with $Ca_V1.1a$. Because the effect of the IVS3-S4 linker was more pronounced near the extracellular side of the VSD, we also measured the distance between the R1, R2, and R3 charges and a negatively charged residue (D4 = D1196) further outside in IVS3. Here the models show an increase of the distance in the resting state and in both intermediate states and a reduced distance in the activated state of $Ca_V1.1e$ relative to $Ca_V1.1a$. The increased variability between clusters of the same variant and between variants are expected to alter the transient H-bond formation between IVS4-positive charges and potential counter charges in IVS2 and IVS3 during the sequential steps of the voltage-sensing process.

In the resting state of both $Ca_V1.1$ variants (Figure 3A), the outer arginines of IVS4 (R1 and R2) reside in the CTC forming H-bonds with D3. A smaller number of H-bonds and distances >2 Å indicate weaker interactions in $Ca_V1.1a$. The outer aspartate D4 resides near arginine (R0) at the extracellular end of the IVS4 helix, and three of the five top model clusters indicate an

Table 1. Distance Measurements between C^{α} of S4 Charged Amino Acids and Different Amino Acids from S2 and S3 during Gating

		F-R1	*E2-R1*	*D3-R1*	*D4-R0*
Resting state	**$Ca_V1.1a$**	10.63 ± 0.00	12.44 ± 0.00	6.23 ± 0.00	7.50 ± 0.30[a]
	$Ca_V1.1e$	10.63 ± 0.00	12.44 ± 0.00	6.23 ± 0.00	8.01 ± 0.37[a]
		F-R2	*E2-R2*	*D3-R2*	*D4-R0*
Intermediate State 1	**$Ca_V1.1a$**	10.55 ± 0.30	12.13 ± 0.45	6.39 ± 0.40	5.52 ± 0.33[a]
	$Ca_V1.1e$	10.47 ± 0.24	12.08 ± 0.29	6.23 ± 0.00	6.23 ± 0.47[a]
		F-R3	*E2-R3*	*D3-R3*	*D4-R1*
Intermediate State 2	**$Ca_V1.1a$**	10.86 ± 0.36[b]	12.73 ± 0.67[b]	6.61 ± 0.21[a]	6.81 ± 0.68[a]
	$Ca_V1.1e$	10.64 ± 0.08[b]	12.17 ± 0.15[b]	6.83 ± 0.20[a]	7.24 ± 0.76[a]
		F-K4	*E2-K4*	*D3-K4*	*D4-R1*
Activated State	**$Ca_V1.1a$**	10.29 ± 0.17	12.05 ± 0.24	5.83 ± 0.18[a]	5.89 ± 0.16[b]
	$Ca_V1.1e$	10.21 ± 0.34	11.86 ± 0.60	6.04 ± 0.24[a]	5.67 ± 0.22[b]

All distances are expressed in Ångström (Å) ± SD. The exact amino acid in the fourth VSD of $Ca_V1.1$ are: F=F1161, E2= E1164, D3=D1186, D4=D1196, R0=R1229 ($Ca_V1.1a$) or R1210 ($Ca_V1.1e$), R1=R1236 ($Ca_V1.1a$) or R1217 ($Ca_V1.1e$), R2=R1239 ($Ca_V1.1a$) or R1220 ($Ca_V1.1e$), R3=R1242 ($Ca_V1.1a$) or R1223 ($Ca_V1.1e$), K4=K1245 ($Ca_V1.1a$) or K1226 ($Ca_V1.1e$).

[a]The difference in distance (of at least 0.2 Å) if the distance is larger in $Ca_V1.1e$ compared with $Ca_V1.1a$.

[b]The difference in distance (of at least 0.2 Å) if the distance is larger in $Ca_V1.1a$ compared with $Ca_V1.1e$.

H-bond between R0 and D4 in $Ca_V1.1e$. In the intermediate state 1 (Figure 3B), the number and length of the H-bonds of R0, R1, and R2 and partners in IVS2 and IVS3 are very similar in both splice variants. However, in the intermediate state 2 (Figure 3C), the changed distances between the transmembrane helices of $Ca_V1.1a$ or $Ca_V1.1e$ profoundly affect H-bond formation especially between D4 and R1. Whereas in $Ca_V1.1a$ only two of the top five clusters form H-bonds between R1 and D4 in IVS3, the $Ca_V1.1e$ models indicate stronger interactions between these two residues (Table S1 related to Figures 3 and 4). In three of the top five analyzed clusters, R1 forms two H-bonds with D4 and, in one cluster, one H-bond. In the activated state of both $Ca_V1.1e$ and $Ca_V1.1a$ (Figure 3D), D4 forms H-bonds with the next arginine of the IVS4 helix, R2. However, overall the number of D4-R2 H-bonds is higher and their distance shorter in the models of $Ca_V1.1e$ compared with $Ca_V1.1a$, consistent with stronger interactions in $Ca_V1.1e$. In addition, in two of the five top $Ca_V1.1e$ clusters, also the interaction between R1 and D4 is maintained in the activated state. This is not found in any of the $Ca_V1.1a$ models, in which R0 and R1 form several H-bonds with different acceptors in IVS3. Collectively our modeling indicates that, in $Ca_V1.1e$ stronger, R1-D4 interactions in the intermediate state 2 may facilitate the transition toward activation, thus increasing the voltage sensitivity. The multiple interactions of both R1 and R2 with D4 may stabilize the voltage sensor of $Ca_V1.1e$ in the activated state, possibly causing the increased $Ca_V1.1e$ channel current amplitude. Therefore, we hypothesize that the aspartate D1196 (D4) is a critical residue for voltage sensing of $Ca_V1.1$ channels, potentially involved in facilitating the transition from intermediate state 2 to activation, and in stabilizing the activated state of the $Ca_V1.1e$ splice variant.

Site-Directed Mutagenesis Confirms the Importance of D1196 for Determining the Voltage Sensitivity of $Ca_V1.1e$

To test the hypothesis that D4 is a critical determinant of the distinct voltage sensitivities and current amplitude of $Ca_V1.1$ variants, we neutralized the charge of the aspartate D1196 by mutating it to asparagine in both splice variants. We expressed wild-type and mutant GFP-tagged $Ca_V1.1a$ or $Ca_V1.1e$ constructs in dysgenic ($Ca_V1.1$-null) myotubes and analyzed their current properties using whole-cell patch-clamp recording. Wild-type $Ca_V1.1e$ showed a 6- to 8-fold increased calcium current amplitude and a 26-mV left shift in the voltage dependence of current activation compared with full-length $Ca_V1.1a$, as previously described (Tuluc et al., 2009) (Figures 4A–4C; Table 2). Consistent with the structural modeling predictions, neutralizing the negatively charged D4 in $Ca_V1.1e$ ($Ca_V1.1e$-D4N) reversed the effects of exon 29 exclusion almost completely. Its voltage dependence of activation was right shifted by 19 mV, and the peak amplitude was reduced to about the same level as that of $Ca_V1.1a$. In contrast, the identical mutation in the full-length $Ca_V1.1a$ ($Ca_V1.1a$-D4N) had no effect on voltage dependence, and only a small effect on the current amplitude. Thus, D1196 (D4) is essential for the characteristic gating properties of the $Ca_V1.1e$ channel by acting as counter charge for IVS4 gating charges, but it does not contribute substantially to the gating of $Ca_V1.1a$.

To examine whether the negative charge or the predicted H-bonds of the D1196 are critical for the leftwards shift in the voltage sensitivity of $Ca_V1.1e$, we generated a second mutant in which the aspartate was substituted by the negatively charged but longer side-chain glutamate ($Ca_V1.1e$-D4E). Interestingly, this mutation ($Ca_V1.1e$-D4E) also reduced the voltage sensitivity and current amplitude to values near those of $Ca_V1.1a$ (Figures 4D–4F). Evidently the presence of the negatively charged carboxyl group at D4 is not sufficient to left shift the voltage sensitivity of $Ca_V1.1e$, but it also has to be positioned at the exact distance from the protein backbone to properly interact with the basic side chain of the arginines in IVS4.

To further examine this possibility, we modeled $Ca_V1.1e$-D4E in the four different conformational states and compared it with $Ca_V1.1e$. Indeed, structural modeling indicated that mutating the aspartate to glutamate at position 1196 in $Ca_V1.1e$ may well reduce the H-bonds transiently formed with R1, especially in the intermediate state 2 (Table S1 and Figure S2 related to

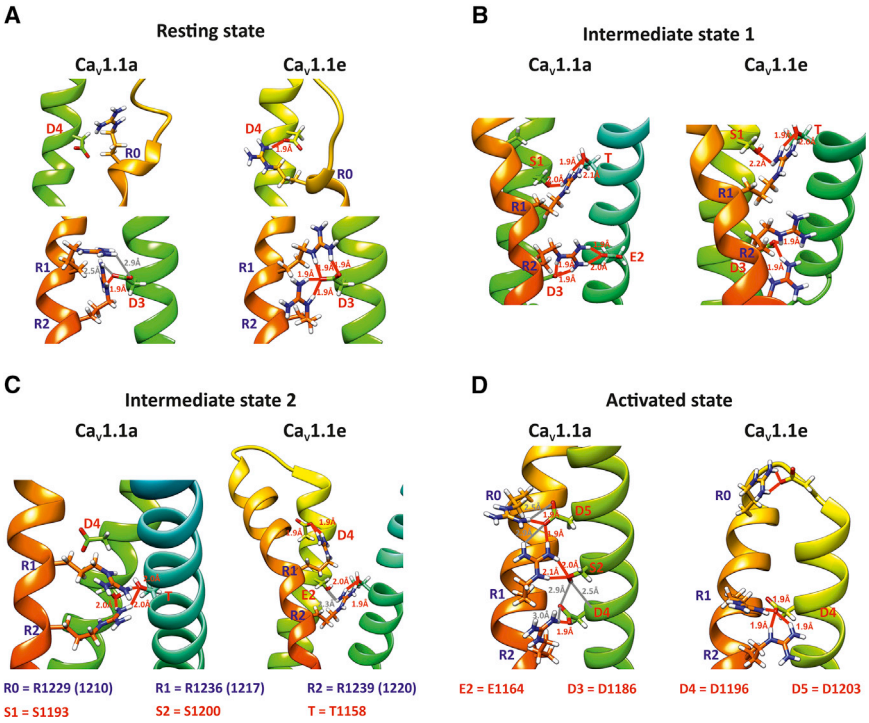

Figure 3. Structural Differences in the Fourth VSD of $Ca_V1.1e$ and $Ca_V1.1a$ Affect the Number and Strengths of H-bonds Sequentially Formed During Gating

(A) In the resting state, R1 and R2 of $Ca_V1.1e$ form several H-bonds with D3 with distances $\leq$2 Å, while $Ca_V1.1a$ R1 and R2 interaction with D3 results in less and weaker H-bonds. An additional arginine on the extracellular side of IVS4 (R0) forms one H-bond with an IVS3 aspartate (D4) in $Ca_V1.1e$ but not in $Ca_V1.1a$.

(B) H-bonds in intermediate state 1 are similar in both splice variants.

(C) In intermediate state 2, R1 of $Ca_V1.1e$ interacts with D4, and R2 with E2 and T, while in $Ca_V1.1a$, both R1 and R2 interact exclusively with E2 and T.

(D) The activated state of $Ca_V1.1e$ is characterized by multiple interactions of R1 and R2 with D4, while R0, R1, and R2 of $Ca_V1.1a$ form interactions with different H-bond acceptors from IVS3 (D4, D4, S2). The H-bonds and their distances are illustrated using UCSF Chimera (Pettersen et al., 2004). Relevant H-bonds <2.0 Å are colored in red while distances >2.0 Å are shown in gray.

Figures 3 and 4). Whereas in $Ca_V1.1e$ four of five clusters R1 interacted with D4 (three clusters two H-bonds and one cluster one H-bond) in $Ca_V1.1$-D4E, the number of clusters showing interactions between R1 and E1196 was reduced to one with two H-bonds plus two with a single H-bond. Such a drop in the number of H-bonds and in the fraction of model clusters where these bonds occur is consistent with the experimentally observed shift of the voltage sensitivity toward more depolarizing potentials. Together these mutagenesis experiments and related structural models suggest that D4 facilitates voltage-sensitive transitions by interacting with positive IVS4 charges. This raises the question as to which interactions of D4 with which of the arginines represents the limiting gating transition for current activation?

The Interactions of R1 and R2 with D4 Determine the Voltage Sensitivity of $Ca_V1.1e$

Our structural modeling (Figure 3) indicated that R0, R1, and R2 differentially interact with D4 in $Ca_V1.1e$ compared with $Ca_V1.1a$. To determine which of these putative interactions are important for the ~26-mV left shift in the voltage sensitivity of $Ca_V1.1e$, we mutated R0, R1, or R2 to alanine and analyzed their current properties. According to structural modeling, the outermost arginine R0 forms an H-bond with D4 of $Ca_V1.1e$ but not of $Ca_V1.1a$ in the resting state. Mutation of R0 in $Ca_V1.1e$ ($Ca_V1.1e$-R0A) caused a slight increase in current density and only a 7-mV right shift of the voltage dependence of activation (Figures 5A–5C). These modest effects are very different from the properties of $Ca_V1.1a$ or from the changes effected by mutations of D4. Therefore the R0-D4 interaction is not the major determinant for the specific voltage sensitivity and current amplitude of $Ca_V1.1e$.

Our structural models further predicted that, in the intermediate state 2, R1 forms more H-bonds with D4 in $Ca_V1.1e$, but not in $Ca_V1.1a$, and that this interaction is maintained in the activated state. Thus, the R1-D4 interaction might facilitate the final transition toward activation in $Ca_V1.1e$ and then contribute to the stabilization of the activated state. Consistent with its importance for voltage sensing, mutating R1 in $Ca_V1.1e$ ($Ca_V1.1e$-R1A) caused a substantial right shift (35 mV) of the voltage dependence of activation to even higher voltages than $Ca_V1.1a$ (Figures 5A–5C). Also, the $Ca_V1.1e$-R1A channel shows a decreased current amplitude compared with $Ca_V1.1e$. However, $Ca_V1.1e$-R1A currents are still higher than in $Ca_V1.1a$ and about half of the decline can be explained by the decreased driving force at the higher activation voltages. Overall, neutralizing R1 identifies the R1-D3 interaction as a major determinant of the voltage sensitivity of $Ca_V1.1e$ and reveals a differential role of this interaction in determining the voltage dependence and current amplitude of $Ca_V1.1$.

Finally, our structural modeling indicated that, in the activated state, R2 forms a greater number of H-bonds with D4 in $Ca_V1.1e$ compared with $Ca_V1.1a$. These H-bonds may facilitate the transition to the open state and stabilize the voltage sensor in the activated state, thus shifting the voltage sensitivity toward lower potentials and increasing the amplitude. Indeed, mutation of R2 in $Ca_V1.1e$ ($Ca_V1.1e$-R2A, Figures 5A–5C) reduced the current density and right shifted the voltage dependence by 30 mV adopting current properties identical to those of $Ca_V1.1a$, confirming the importance of the R2-D4 interaction for determining the gating properties of $Ca_V1.1e$.

If R1A and R2A mutations in $Ca_V1.1e$ reverse the facilitating effects of exon 29 deletion, then the corresponding mutations in $Ca_V1.1a$ should not have an additional effect on its current-voltage dependence. Indeed, R1A and R2A mutations in $Ca_V1.1a$ (Figures 5D–5F) did not affect the voltage dependence

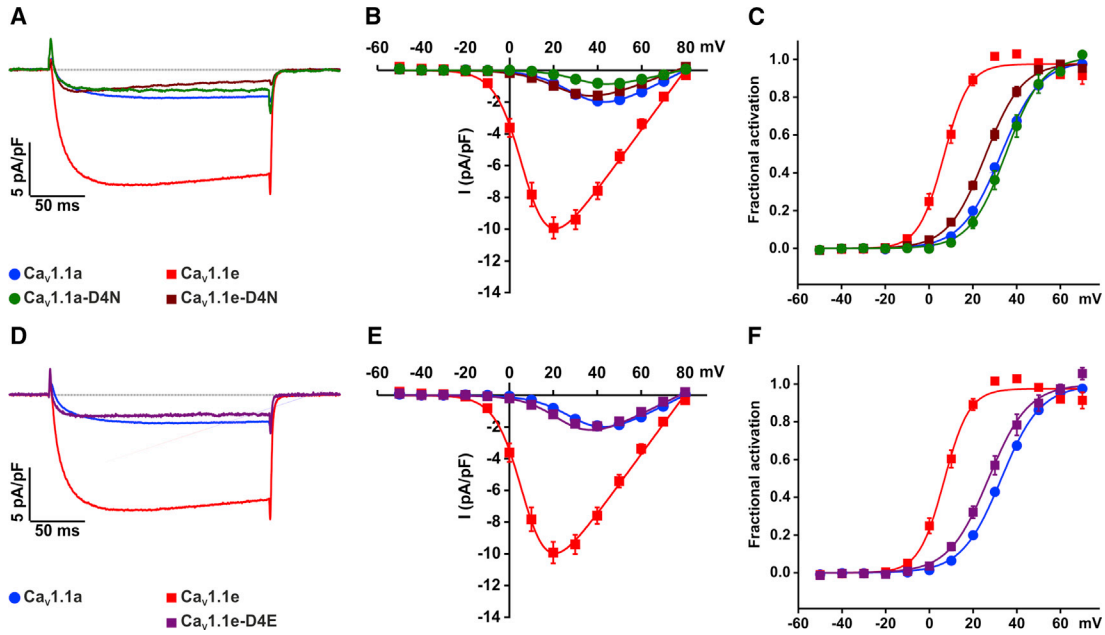

Figure 4. Aspartate at Position 1196 Is Critical in Determining the Voltage Sensitivity of $Ca_V1.1$ but Not $Ca_V1.1a$

(A–C) Representative calcium currents recorded from myotubes expressing $Ca_V1.1a$ (blue), $Ca_V1.1e$ (red), $Ca_V1.1a$-D4N (green), and $Ca_V1.1e$-D4N (wine) during a 200-ms step depolarization to the maximum current amplitude (A). The $Ca_V1.1e$ splice variant has a ~6-fold higher current amplitude and ~26 mV left shift in voltage dependence compared with $Ca_V1.1a$. Mutating the negatively charged aspartate (D4) at position 1196 to the neutral asparagine ($Ca_V1.1e$-D4N, wine) reverts $Ca_V1.1e$ calcium current properties to those of $Ca_V1.1a$, as illustrated by (B) the I/V curve and (C) voltage dependence of current activation. Mutating the same amino acid in $Ca_V1.1a$ ($Ca_V1.1a$-D4N, green) has no effect on voltage sensitivity but slightly reduces the current amplitude.

(D–F) Mutating the $Ca_V1.1e$ aspartate (D4) to a glutamate results in the same reduction in amplitude ($Ca_V1.1e$-D4E, purple) and shift in the voltage dependence as observed for the aspartate to asparagine mutation. All data are presented as means ± SEM. Currents were analyzed as previously described (Tuluc et al., 2007) and the calcium current parameters and statistics are given in Table 2.

of activation. This also excludes the possibility that the effects observed with the corresponding mutations in $Ca_V1.1e$ simply resulted from the reduced number of total charges in the voltage sensor. Only if the voltage sensitivity of the $Ca_V1.1a$ R1A mutation had also been right shifted compared with the wild-type would this have been an indication that R1 interactions with other counter charges besides D4 were responsible for the voltage sensitivity. But this was not the case.

As it stands, the strikingly similar effects of mutating D4, R1, or R2 identify these oppositely charged residues in IVS3 and IVS4 as interaction partners that determine the ~26-mV leftward shift in the voltage sensitivity and the high current amplitude of $Ca_V1.1e$ splice variant. Thus, structure modeling and mutagenesis experiments indicate that inclusion of exon 29 in the IVS3-S4 linker of $Ca_V1.1a$ perturbs interactions between D4 in IVS3 and the two outer IVS4 arginines R1 and R2. This possibly increases the energy necessary for the transition between intermediate state 2 and the activated state and reduces the stability of the activated state.

DISCUSSION

Here we used structural modeling, site-directed mutagenesis and electrophysiology in a native cell system to identify amino acid interactions responsible for charge transfer in the Ca_V channel VSD, which critically determine the gating properties of Ca_V channels. Our study elucidates the role of the extracellular IVS3-S4 linker on the gating mechanism responsible for the dramatic difference in the voltage sensitivity and current amplitude of two naturally occurring $Ca_V1.1$ channel splice variants. The gating behavior of the long $Ca_V1.1a$ splice variant has been a conundrum in the ion channel field for over three decades, because the voltage dependence of its gating currents and of excitation-contraction coupling occurs at about 30 mV lower voltage than the voltage sensitivity of its ionic conductance. Several previous studies demonstrated that the specific slow speed of $Ca_V1.1$ current activation is determined by the S3 segment plus S3-S4 linker in the first repeat (Nakai et al., 1994; Tanabe et al., 1991); nevertheless, the mechanism responsible for the right-shifted voltage sensitivity of $Ca_V1.1a$ ionic current has not been identified. The characterization of the embryonic $Ca_V1.1e$ splice variant (Tuluc et al., 2009), which exhibits the same voltage sensitivity as gating currents, excitation-contraction coupling, and ionic conductance, indicated that the limiting voltage-sensitive step required for $Ca_V1.1$ channel gating occurs in the VSD of the fourth repeat. Therefore, the naturally occurring $Ca_V1.1$ splice variants represent an excellent model to study the voltage sensor transitions responsible for the differential voltage sensitivities of Ca_V channels.

How does the inclusion or exclusion of 19 amino acids encoded by exon 29 in the IVS3-S4 linker cause the striking differences in voltage sensitivity of the two $Ca_V1.1$ splice variants? Conceptually, a very short IVS3-S4 linker in $Ca_V1.1e$ could lock this voltage sensor in the activated position, and consequently

Table 2. Calcium Currents Biophysical Properties

	I_{peak} (pA/pF)	V_{half} (mV)	V_{half} Significance	V_{rev} (mV)	k_{act} (mV)	n
$Ca_V1.1e$	−10.4 ± 0.7	7.0 ± 1.1	–	79.2 ± 1.1	4.7 ± 0.2	27
$Ca_V1.1e$-D4N	−1.6 ± 0.1	26.4 ± 1.0	<0.0001	75.8 ± 1.2	8.8 ± 0.4	16
$Ca_V1.1e$-D4E	−1.9 ± 0.2	27.8 ± 1.7	0.0002	77.6 ± 2.9	9.3 ± 0.9	6
$Ca_V1.1e$-R0A	−12.1 ± 2.3	14.8 ± 2.6	0.0288	83.8 ± 1.2	5.7 ± 0.6	9
$Ca_V1.1e$-R1A	−3.4 ± 0.4	43.9 ± 0.8	<0.0001	82.8 ± 1.4	9.4 ± 0.7	10
$Ca_V1.1e$-R2A	−1.4 ± 0.1	32.3 ± 1.4	<0.0001	72.1 ± 1.3	8.1 ± 0.7	8
$Ca_V1.1a$	−1.9 ± 0.2	33.2 ± 0.8	–	79.8 ± 1.1	8.9 ± 0.3	21
$Ca_V1.1a$-D4N	−0.9 ± 0.2	35.2 ± 1.9	0.4261	76.6 ± 1.9	7.8 ± 0.6	7
$Ca_V1.1a$-R1A	−0.5 ± 0.1	34.8 ± 5.6	0.8614	77.5 ± 3.7	7.7 ± 1.7	3
$Ca_V1.1a$-R2A	−0.4 ± 0.1	37.0 ± 3.9	0.4813	70.7 ± 2.4	7.8 ± 0.5	4

All data are presented as means ± SEM. The significance levels were calculated using the Mann-Whitney U test between each construct and the original channel splice variant used as backbone.

the voltage sensitivity of the channel would be determined by the other three voltage sensors. However, immobilizing one of the four voltage sensors would be expected to result in a measurable reduction of the gating charge currents (Q_{ON}) in $Ca_V1.1e$ compared with $Ca_V1.1a$. This has not been observed in our previous study where the voltage dependence and maximum amplitude of the gating charge currents (Q_{ON}) were found to be identical for both splice variants, while the expression level (determined by RyR calcium release) was equal (Tuluc et al., 2009). Furthermore, here we show that neutralization of R1, R2, or D4 in the fourth VSD of $Ca_V1.1e$ similarly right shifted the voltage dependence of current activation, which is inconsistent with a model assuming a locked fourth voltage sensor.

Alternatively, our structural models of the long IVS3-S4 linker indicate a substantial conformational change between the intermediate state 2 and the activated state. Since voltage-sensing transitions are expected to be very fast, the movement of the extra 19 amino acids encoded by exon 29 away from the outer vestibule could affect the response speed of this voltage sensor and therefore the current activation kinetics. Indeed, in our previous study, we report that $Ca_V1.1e$ currents activate faster than $Ca_V1.1a$ currents (Tuluc et al., 2009). Although we cannot exclude that the structural rearrangement of the IVS3-S4 linker might also increase the energy required to gate this VSD of $Ca_V1.1a$, our experimental finding that mutations of D4 (D4N and D4E) in $Ca_V1.1e$ right shifts the voltage dependence in the absence of exon 29 contradicts this possibility.

Another possibility is that inclusion of exon 29 in the IVS3-S4 linker causes displacement of IVS3 and IVS4 relative to each other and consequently alters the intramolecular interactions required for the transfer of the IVS4 gating charges upon depolarization. Indeed our structural models of the fourth VSD of $Ca_V1.1a$ and $Ca_V1.1e$ reveal differences in the relative positioning of IVS2, IVS3, and IVS4. These differences dramatically affect H-bond formation of several IVS4 arginines, particularly in intermediate state 2 and the activated state. Our experimental results showing that mutations of R1 and R2 in IVS4 or of the pivotal aspartate in IVS3 (D4) of $Ca_V1.1e$ revert voltage sensitivity and current amplitude to values similar to those found in $Ca_V1.1a$ strongly support this model. In Na_V and Kv channels, negatively charged residues in the transmembrane helices S2 (E2) and S3 (D3) and a non-polar residue in S2 (F) form the CTC, which supports the voltage-dependent transition of the positively charged residues in S4 (Payandeh et al., 2011, 2012; Tao et al., 2010). Here we show that the corresponding amino acids in the fourth VSD of $Ca_V1.1$ channels appear to serve the same function but are not much affected by the inclusion of exon 29. Instead we identified a previously unnoticed negatively charged amino acid in IVS3 (D1196), which is essential for proper gating of the $Ca_V1.1e$ channel. Our structural models predict that during the gating process D1196 sequentially interacts with R1 and R2, and that these transitions are dramatically altered by inclusion of exon 29 in $Ca_V1.1a$. Our experimental analysis demonstrates that mutation of D1196 to asparagine or glutamate in $Ca_V1.1e$ reverts both the voltage sensitivity and the current density to that of $Ca_V1.1a$. Thus, D1196 is the key determinant of the dramatically different gating properties of the two $Ca_V1.1$ splice variants. Moreover, mutational analysis of the IVS4 arginines confirms the importance of D1196 interactions with R1 and R2 in determining the leftward shift by 26 mV of $Ca_V1.1e$ voltage sensitivity. Thus, in $Ca_V1.1$ channels, an additional charged residue in IVS3 contributes to S4 charge compensation, and deviations of its relative position to IVS4 accomplish dramatic changes of the channel's voltage sensitivity and current amplitude.

Our experimental data support a model according to which the interactions of R1 and R2 with D4 contribute to the final steps of the charge transfer to different degrees in $Ca_V1.1a$ and $Ca_V1.1e$. In the intermediate state 2 of $Ca_V1.1a$, both R1 and R2 form H-bonds with a single residue in IVS2 (T). Although these interactions might stabilize this state, our experimental data showing that neutralization of R1 or R2 does not improve $Ca_V1.1a$ gating do not support this notion. In contrast, in the intermediate state 2 of $Ca_V1.1e$, the R1-D4 interaction (Figure 3C) most probably facilitates the final transition to the activated state as the mutation of R1 in $Ca_V1.1e$ shifts its voltage sensitivity to the right to potentials even higher than $Ca_V1.1a$. The notion that $Ca_V1.1a$ R1 and D4 do not interact is supported by our data showing that, in $Ca_V1.1a$, neutralization of R1 or D4 does not alter the voltage dependence. In the activated state, R1 and R2 of $Ca_V1.1a$ form H-bonds with three separate IVS3 residues, whereas, in $Ca_V1.1e$, both R1 and R2 form multiple H-bonds with D4 (Figure 3D). This convergence on a single residue most probably

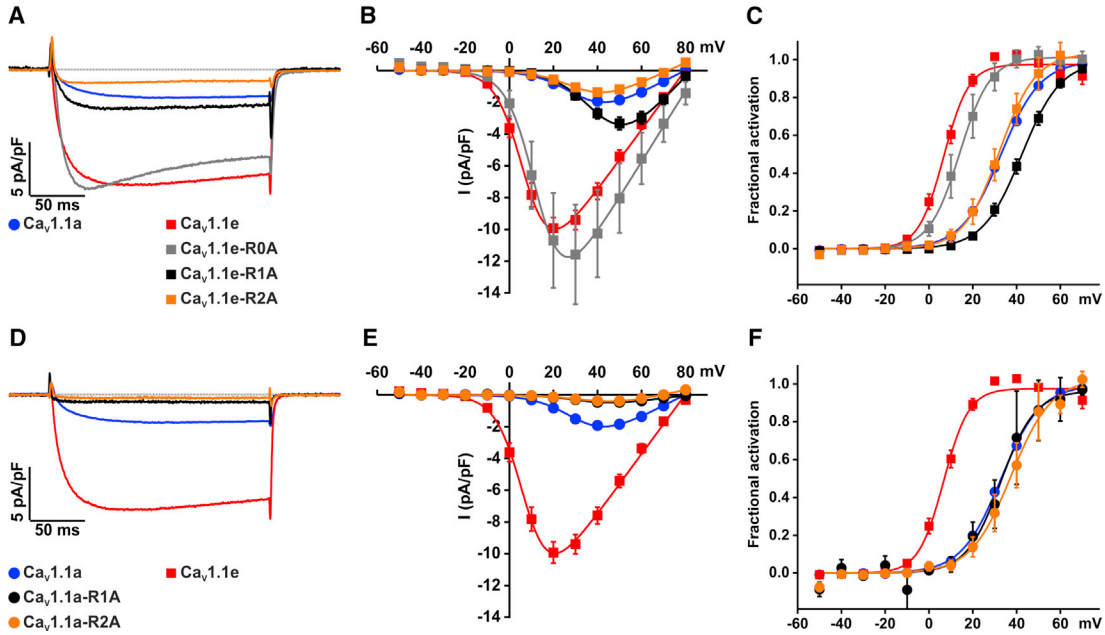

Figure 5. R1 and R2 Are Functionally Relevant Interaction Partners for D4 in $Ca_V1.1e$ but Not in $Ca_V1.1a$

(A) Representative calcium currents recorded during a 200-ms step depolarization to the maximum current amplitude from myotubes expressing $Ca_V1.1a$ (blue), $Ca_V1.1e$ (red), or $Ca_V1.1e$ with arginine-to-alanine mutations of R0 ($Ca_V1.1e$-R0A, gray), R1 ($Ca_V1.1e$-R1A, black), and R2 ($Ca_V1.1e$-R2A, orange).

(B and C) Neutralizing R2 of $Ca_V1.1e$ ($Ca_V1.1e$-R2A) converts the amplitude and voltage-dependence of $Ca_V1.1e$ to that of $Ca_V1.1a$. R1 neutralization in $Ca_V1.1e$ ($Ca_V1.1e$-R1A) elicits an even further right-shifted voltage dependence compared with $Ca_V1.1a$. In contrast, R0 neutralization of $Ca_V1.1e$ ($Ca_V1.1e$-R0A) shifts the voltage dependence of $Ca_V1.1e$ by only ~7 mV to the right and slightly increases the current amplitude.

(D–F) Neutralizing R1 and R2 charges in $Ca_V1.1a$ ($Ca_V1.1a$-R1A, black and $Ca_V1.1a$-R2A, orange) does not affect the voltage dependence, but results in reduced calcium current amplitude. All data are presented as means ± SEM. The recording conditions and analysis were identical to those described in the legend of Figure 4. The calcium current parameters and statistics are given in Table 2.

stabilizes the activated state resulting in the observed higher current density of $Ca_V1.1e$. Our experimental data showing that, in the absence of the R1-D4 interactions in $Ca_V1.1e$-R1A, the current amplitude is substantially higher than that of $Ca_V1.1a$ (Figure 5B) confirms that the stronger R2-D4 interaction in $Ca_V1.1e$ significantly contributes to the stability of the open state.

Our current and previous observation that the deletion of exon 29 dramatically alters the voltage dependence and amplitude of $Ca_V1.1a$ calcium currents demonstrates that voltage-sensitive transitions in the fourth repeat VSD are necessary for $Ca_V1.1$ channel opening, but are not sufficient. As has been previously shown, our data also support the idea that gating of the calcium channel requires different contributions from all VSDs (Beyl et al., 2012; Dirksen et al., 1997; Garcia et al., 1997; Hamid et al., 2006; Hohaus et al., 2005; Kudrnac et al., 2009; Li et al., 2004; Nakai et al., 1994; Pantazis et al., 2014; Tanabe et al., 1991; Wall-Lacelle et al., 2011). Recently published voltage-clamp fluorometry experiments demonstrate that, in the $Ca_V1.2$ channel, VSD II and III control the channel opening with no apparent contribution of the fourth VSD (Pantazis et al., 2014). Nevertheless, this does not exclude the possibility that alternative splicing in the fourth VSD of $Ca_V1.2$ would change the contribution of this VSD to channel gating. Our data support a gating model according to which the transitions of the first three VSDs and the early transitions of the fourth VSD are similar in both $Ca_V1.1$ variants, but, in the $Ca_V1.1a$ variant, the final transitions of the fourth VSD require more energy and thus determine the voltage sensitivity of channel activation. The voltage dependence of channel gating in the $Ca_V1.1e$ variant is probably determined by the other VSDs similarly to the $Ca_V1.2$ channel previously described (Pantazis et al., 2014). The quantification of the slope factor (k_{act} see Table 2) of the Bolzmann fit to the voltage dependence of the conductance (Bezanilla, 2000; Noceti et al., 1996) also supports our model that the critical difference between $Ca_V1.1$ variants is the final gating of the fourth VSD, because the slope factor of $Ca_V1.1a$ mirrors the movement of ~3.2 charges, whereas the slope factor for $Ca_V1.1e$ channel mirrors the movement of ~5.4 charges. Previous evidence supports a cooperative gating model for Ca_V channels according to which the VSDs have different contributions to channel opening and affect each other (Beyl et al., 2012; Demers-Giroux et al., 2013; Pantazis et al., 2014). Whether the increased number of charges responsible for gating in $Ca_V1.1e$ reflect the biophysical changes in the fourth VSD alone or altered gating of the other VSDs remains to be further studied.

Together our structural modeling and mutagenesis data identified a molecular mechanism in the fourth VSD of $Ca_V1.1$ channels that explains the specific current amplitude and voltage sensitivity of this L-type Ca_V channel. The molecular mechanism hinges on the newly discovered interaction between D4 and two IVS4 arginines, and it is exquisitely sensitive to structural rearrangements between the IVS3 and IVS4 helices imposed by alternative splicing of the IVS3-S4 linker. Importantly, the D4 aspartate is highly conserved in the fourth VSD of all high voltage-activated Ca_V channels (Figure S1 related to Figure 1).

Because all but one *CACNA1* gene encoding Ca_V channels also contain a physiologically relevant alternative splicing site in the extracellular IVS3-S4 linker of this domain (Lipscombe et al., 2013), the molecular mechanism described here may be relevant for fine-tuning the voltage sensitivity throughout the Ca_V channel family.

EXPERIMENTAL PROCEDURES

Structural Modeling

Homology, de novo, and full-atom modeling of the $Ca_V1.1e$ and $Ca_V1.1a$ VSDs was performed using the Rosetta-Membrane method (Yarov-Yarovoy et al., 2006a, 2006b, 2012) and Na_VAb VSD structure (Payandeh et al., 2011) as a template. For modeling of resting and intermediate states, we used multiple alignments between S4 segments of $Ca_V1.1e$ or $Ca_V1.1a$ and Na_VAb guided by experimental data on specific pairwise interactions and positions of S4 arginines in different states of K_V and Na_V VSDs (Broomand and Elinder, 2008; Campos et al., 2007; DeCaen et al., 2008, 2009, 2011; Henrion et al., 2012; Lacroix et al., 2014; Pathak et al., 2007; Starace and Bezanilla, 2004; Tombola et al., 2005; Vargas et al., 2012; Yarov-Yarovoy et al., 2012). The S4 alignment where R1 in $Ca_V1.1$ variants is aligned to R1 in Na_VAb represents the activated state. The intermediate state 2, intermediate state 1, and resting state were modeled by aligning R1 in $Ca_V1.1$ variants to Na_VAb R2, R3, and R4 respectively. In the resting state, the CTC is occupied by R1 ($Ca_V1.1a$-R1236; $Ca_V1.1e$-R1217); in the intermediate state 1 by R2 ($Ca_V1.1a$-R1239; $Ca_V1.1e$-R1220), and in the intermediate state 2 by R3 (R1242-$Ca_V1.1a$; $Ca_V1.1e$-R1223). In the activated state, K4 ($Ca_V1.1a$-K1245; $Ca_V1.1e$-K1226) occupies the CTC. The S1-S2, S2-S3, and S3-S4 loops were built using Rosetta cyclic coordinate descent and kinematic closure loop modeling applications (Mandell et al., 2009; Wang et al., 2007), and guided by membrane environment specific energy function (Barth et al., 2007; Yarov-Yarovoy et al., 2012). A total of 10,000 models were generated for each state and ranked by total Rosetta score (Barth et al., 2007; Rohl et al., 2004; Yarov-Yarovoy et al., 2012). The top 10% of best scoring models are clustered (Bonneau et al., 2002) using the root mean square deviation threshold, which generates at least 150–200 models in the largest cluster. Models representing centers of the top 20 clusters were used as inputs for full-atom relax. Models representing five largest clusters for each of the VSD states were chosen for further visual evaluation and analysis. All structural figures in the article were generated using UCSF Chimera (Pettersen et al., 2004).

Mutagenesis and Electrophysiology

The point mutations were introduced using splicing by overhang extension PCR into the GFP-α_{1S} or GFP-α_{1S}-ΔE29 plasmids previously described (Tuluc et al., 2009). All mutants were verified by sequencing performed by Eurofins Genomis. The plasmids were transfected in myotubes of the dysgenic (mdg/mdg) cell line GLT using FuGene transfection reagent (Roche Diagnostics) (Tuluc et al., 2007). This restores the normal composition of the channel with auxiliary $\alpha_2\delta$-1, β_{1a}, and γ_1 subunits enabling recording of the otherwise undetectable $Ca_V1.1a$ currents (Flucher et al., 2005; Rios and Brum, 1987; Tanabe et al., 1988). Calcium currents were recorded with the ruptured whole-cell patch-clamp technique in voltage-clamp mode using an Axopatch 200B amplifier (Axon Instruments). Patch pipettes (borosilicate glass, Harvard Apparatus) had a resistance of 1.5–3 MΩ when filled with 145 mM Cs-aspartate, 2 mM $MgCl_2$, 10 mM HEPES, 0.1 mM Cs-EGTA, 2 mM Mg-ATP (pH 7.4 with CsOH). The bath solution contained 10 mM $CaCl_2$, 145 mM tetra-ethyl ammonium chloride, 10 mM HEPES (pH 7.4 with tetra-ethyl ammonium hydroxide). Data acquisition and command potentials were controlled by pClamp software (version 8.0; Axon Instruments); analysis was performed using Clampfit 8.0 (Axon Instruments) and SigmaPlot 8.0 (SPSS Science) software. The current-voltage dependence was fitted according to: $I = G_{max} \cdot (V - V_{rev})/1(1 + \exp(-(V - V_{1/2})/(k))$. The conductance was calculated using $G = (-I * 1000)/(V - V_{rev})$ and its voltage dependence was fitted according to a Boltzmann distribution: $G = G_{max}/(1 + \exp(-(V - V_{1/2})/k_{act}))$, where G_{max} is the maximum conductance of the L-type calcium currents, V_{rev} is the extrapolated reversal potential of the calcium current, $V_{1/2}$ is the potential for half maximal conductance, and k_{act} is the slope. The statistical significance was calculated using the Mann-Whitney U test, and the values are present in Table 2.

SUPPLEMENTAL INFORMATION

Supplemental Information includes two figures, one table, and two movies and can be found with this article online at http://dx.doi.org/10.1016/j.str.2015.11.011.

AUTHOR CONTRIBUTIONS

Conceptualization, P.T. and B.E.F.; methodology, P.T. and V.Y-Y.; investigation, P.T., V.Y.-Y., B.B., and B.E.F.; formal analysis, P.T. and B.B.; writing the original draft, P.T., V.Y.-Y., B.B., and B.E.F.; Writing, review, and editing, P.T. and B.E.F.; visualization, P.T. and B.B.; funding acquisition, P.T. and B.E.F.

ACKNOWLEDGMENTS

We thank A. Benedetti, R. Egger, and Dr. M. Campiglio for excellent technical support. This study was funded by grants from the Austrian Science Fund (FWF) P23479 and F4406 to B.E.F., and from the University of Innsbruck P7400-027-011 and P7400-027-012 to P.T.

Received: May 28, 2015
Revised: November 12, 2015
Accepted: November 13, 2015
Published: December 31, 2015

REFERENCES

Ahern, C.A., and Horn, R. (2004). Stirring up controversy with a voltage sensor paddle. Trends Neurosci. *27*, 303–307.

Barth, P., Schonbrun, J., and Baker, D. (2007). Toward high-resolution prediction and design of transmembrane helical protein structures. Proc. Natl. Acad. Sci. USA *104*, 15682–15687.

Beyl, S., Depil, K., Hohaus, A., Stary-Weinzinger, A., Linder, T., Timin, E., and Hering, S. (2012). Neutralisation of a single voltage sensor affects gating determinants in all four pore-forming S6 segments of Ca(V)1.2: a cooperative gating model. Pflugers Arch. *464*, 391–401.

Bezanilla, F. (2000). The voltage sensor in voltage-dependent ion channels. Physiol. Rev. *80*, 555–592.

Bezanilla, F., Perozo, E., Papazian, D.M., and Stefani, E. (1991). Molecular basis of gating charge immobilization in Shaker potassium channels. Science *254*, 679–683.

Bonneau, R., Strauss, C.E., Rohl, C.A., Chivian, D., Bradley, P., Malmstrom, L., Robertson, T., and Baker, D. (2002). De novo prediction of three-dimensional structures for major protein families. J. Mol. Biol. *322*, 65–78.

Broomand, A., and Elinder, F. (2008). Large-scale movement within the voltage-sensor paddle of a potassium channel-support for a helical-screw motion. Neuron *59*, 770–777.

Campos, F.V., Chanda, B., Roux, B., and Bezanilla, F. (2007). Two atomic constraints unambiguously position the S4 segment relative to S1 and S2 segments in the closed state of Shaker K channel. Proc. Natl. Acad. Sci. USA *104*, 7904–7909.

Catterall, W.A. (2010). Ion channel voltage sensors: structure, function, and pathophysiology. Neuron *67*, 915–928.

Catterall, W.A. (2011). Voltage-gated calcium channels. Cold Spring Harb. Perspect. Biol. *3*, a003947.

Catterall, W.A., and Yarov-Yarovoy, V. (2010). Helical motion of an S4 voltage sensor revealed by gating pore currents. Channels (Austin) *4*, 75–77.

Cheng, Y.M., Hull, C.M., Niven, C.M., Qi, J., Allard, C.R., and Claydon, T.W. (2013). Functional interactions of voltage sensor charges with an S2 hydrophobic plug in hERG channels. J. Gen. Physiol. *142*, 289–303.

DeCaen, P.G., Yarov-Yarovoy, V., Zhao, Y., Scheuer, T., and Catterall, W.A. (2008). Disulfide locking a sodium channel voltage sensor reveals ion pair formation during activation. Proc. Natl. Acad. Sci. USA *105*, 15142–15147.

DeCaen, P.G., Yarov-Yarovoy, V., Sharp, E.M., Scheuer, T., and Catterall, W.A. (2009). Sequential formation of ion pairs during activation of a sodium channel voltage sensor. Proc. Natl. Acad. Sci. USA *106*, 22498–22503.

DeCaen, P.G., Yarov-Yarovoy, V., Scheuer, T., and Catterall, W.A. (2011). Gating charge interactions with the S1 segment during activation of a Na+ channel voltage sensor. Proc. Natl. Acad. Sci. USA *108*, 18825–18830.

Demers-Giroux, P.O., Bourdin, B., Sauve, R., and Parent, L. (2013). Cooperative activation of the T-type CaV3.2 channel: interaction between domains II and III. J. Biol. Chem. *288*, 29281–29293.

Dirksen, R.T., Nakai, J., Gonzalez, A., Imoto, K., and Beam, K.G. (1997). The S5-S6 linker of repeat I is a critical determinant of L-type Ca2+ channel conductance. Biophys. J. *73*, 1402–1409.

Flucher, B.E., Obermair, G.J., Tuluc, P., Schredelseker, J., Kern, G., and Grabner, M. (2005). The role of auxiliary dihydropyridine receptor subunits in muscle. J. Muscle Res. Cell Motil. *26*, 1–6.

Flucher, B.E., and Tuluc, P. (2011). A new L-type calcium channel isoform required for normal patterning of the developing neuromuscular junction. Channels (Austin) *5*, 518–524.

Garcia, J., Nakai, J., Imoto, K., and Beam, K.G. (1997). Role of S4 segments and the leucine heptad motif in the activation of an L-type calcium channel. Biophys. J. *72*, 2515–2523.

Hamid, J., Peloquin, J.B., Monteil, A., and Zamponi, G.W. (2006). Determinants of the differential gating properties of Cav3.1 and Cav3.3 T-type channels: a role of domain IV? Neuroscience *143*, 717–728.

Henrion, U., Renhorn, J., Borjesson, S.I., Nelson, E.M., Schwaiger, C.S., Bjelkmar, P., Wallner, B., Lindahl, E., and Elinder, F. (2012). Tracking a complete voltage-sensor cycle with metal-ion bridges. Proc. Natl. Acad. Sci. USA *109*, 8552–8557.

Hohaus, A., Beyl, S., Kudrnac, M., Berjukow, S., Timin, E.N., Marksteiner, R., Maw, M.A., and Hering, S. (2005). Structural determinants of L-type channel activation in segment IIS6 revealed by a retinal disorder. J. Biol. Chem. *280*, 38471–38477.

Kontis, K.J., and Goldin, A.L. (1997). Sodium channel inactivation is altered by substitution of voltage sensor positive charges. J. Gen. Physiol. *110*, 403–413.

Kudrnac, M., Beyl, S., Hohaus, A., Stary, A., Peterbauer, T., Timin, E., and Hering, S. (2009). Coupled and independent contributions of residues in IS6 and IIS6 to activation gating of CaV1.2. J. Biol. Chem. *284*, 12276–12284.

Lacroix, J.J., Hyde, H.C., Campos, F.V., and Bezanilla, F. (2014). Moving gating charges through the gating pore in a Kv channel voltage sensor. Proc. Natl. Acad. Sci. USA *111*, E1950–E1959.

Li, J., Stevens, L., Klugbauer, N., and Wray, D. (2004). Roles of molecular regions in determining differences between voltage dependence of activation of CaV3.1 and CaV1.2 calcium channels. J. Biol. Chem. *279*, 26858–26867.

Liao, P., Yong, T.F., Liang, M.C., Yue, D.T., and Soong, T.W. (2005). Splicing for alternative structures of Cav1.2 Ca2+ channels in cardiac and smooth muscles. Cardiovasc. Res. *68*, 197–203.

Lin, M.C., Hsieh, J.Y., Mock, A.F., and Papazian, D.M. (2011). R1 in the Shaker S4 occupies the gating charge transfer center in the resting state. J. Gen. Physiol. *138*, 155–163.

Lipscombe, D., Andrade, A., and Allen, S.E. (2013). Alternative splicing: functional diversity among voltage-gated calcium channels and behavioral consequences. Biochim. Biophys. Acta *1828*, 1522–1529.

Ma, Z., Lou, X.J., and Horrigan, F.T. (2006). Role of charged residues in the S1-S4 voltage sensor of BK channels. J. Gen. Physiol. *127*, 309–328.

Mandell, D.J., Coutsias, E.A., and Kortemme, T. (2009). Sub-angstrom accuracy in protein loop reconstruction by robotics-inspired conformational sampling. Nat. Methods *6*, 551–552.

Nakai, J., Adams, B.A., Imoto, K., and Beam, K.G. (1994). Critical roles of the S3 segment and S3-S4 linker of repeat I in activation of L-type calcium channels. Proc. Natl. Acad. Sci. USA *91*, 1014–1018.

Noceti, F., Baldelli, P., Wei, X., Qin, N., Toro, L., Birnbaumer, L., and Stefani, E. (1996). Effective gating charges per channel in voltage-dependent K+ and Ca2+ channels. J. Gen. Physiol. *108*, 143–155.

Pantazis, A., Savalli, N., Sigg, D., Neely, A., and Olcese, R. (2014). Functional heterogeneity of the four voltage sensors of a human L-type calcium channel. Proc. Natl. Acad. Sci. USA *111*, 18381–18386.

Papazian, D.M., Timpe, L.C., Jan, Y.N., and Jan, L.Y. (1991). Alteration of voltage-dependence of Shaker potassium channel by mutations in the S4 sequence. Nature *349*, 305–310.

Pathak, M.M., Yarov-Yarovoy, V., Agarwal, G., Roux, B., Barth, P., Kohout, S., Tombola, F., and Isacoff, E.Y. (2007). Closing in on the resting state of the shaker k(+) channel. Neuron *56*, 124–140.

Payandeh, J., Scheuer, T., Zheng, N., and Catterall, W.A. (2011). The crystal structure of a voltage-gated sodium channel. Nature *475*, 353–358.

Payandeh, J., Gamal El-Din, T.M., Scheuer, T., Zheng, N., and Catterall, W.A. (2012). Crystal structure of a voltage-gated sodium channel in two potentially inactivated states. Nature *486*, 135–139.

Pettersen, E.F., Goddard, T.D., Huang, C.C., Couch, G.S., Greenblatt, D.M., Meng, E.C., and Ferrin, T.E. (2004). UCSF Chimera–a visualization system for exploratory research and analysis. J. Comput. Chem. *25*, 1605–1612.

Pless, S.A., Galpin, J.D., Niciforovic, A.P., and Ahern, C.A. (2011). Contributions of counter-charge in a potassium channel voltage-sensor domain. Nat. Chem. Biol. *7*, 617–623.

Pless, S.A., Elstone, F.D., Niciforovic, A.P., Galpin, J.D., Yang, R., Kurata, H.T., and Ahern, C.A. (2014). Asymmetric functional contributions of acidic and aromatic side chains in sodium channel voltage-sensor domains. J. Gen. Physiol. *143*, 645–656.

Rios, E., and Brum, G. (1987). Involvement of dihydropyridine receptors in excitation-contraction coupling in skeletal muscle. Nature *325*, 717–720.

Rohl, C.A., Strauss, C.E., Misura, K.M., and Baker, D. (2004). Protein structure prediction using Rosetta. Methods Enzymol. *383*, 66–93.

Seoh, S.A., Sigg, D., Papazian, D.M., and Bezanilla, F. (1996). Voltage-sensing residues in the S2 and S4 segments of the Shaker K+ channel. Neuron *16*, 1159–1167.

Starace, D.M., and Bezanilla, F. (2004). A proton pore in a potassium channel voltage sensor reveals a focused electric field. Nature *427*, 548–553.

Tanabe, T., Adams, B.A., Numa, S., and Beam, K.G. (1991). Repeat I of the dihydropyridine receptor is critical in determining calcium channel activation kinetics. Nature *352*, 800–803.

Tanabe, T., Beam, K.G., Powell, J.A., and Numa, S. (1988). Restoration of excitation-contraction coupling and slow calcium current in dysgenic muscle by dihydropyridine receptor complementary DNA. Nature *336*, 134–139.

Tao, X., Lee, A., Limapichat, W., Dougherty, D.A., and MacKinnon, R. (2010). A gating charge transfer center in voltage sensors. Science *328*, 67–73.

Tombola, F., Pathak, M.M., and Isacoff, E.Y. (2005). Voltage-sensing arginines in a potassium channel permeate and occlude cation-selective pores. Neuron *45*, 379–388.

Tuluc, P., and Flucher, B.E. (2011). Divergent biophysical properties, gating mechanisms, and possible functions of the two skeletal muscle Ca(V)1.1 calcium channel splice variants. J. Muscle Res. Cell Motil. *32*, 249–256.

Tuluc, P., Kern, G., Obermair, G.J., and Flucher, B.E. (2007). Computer modeling of siRNA knockdown effects indicates an essential role of the Ca2+ channel alpha2delta-1 subunit in cardiac excitation-contraction coupling. Proc. Natl. Acad. Sci. USA *104*, 11091–11096.

Tuluc, P., Molenda, N., Schlick, B., Obermair, G.J., Flucher, B.E., and Jurkat-Rott, K. (2009). A CaV1.1 Ca2+ channel splice variant with high conductance and voltage-sensitivity alters EC coupling in developing skeletal muscle. Biophys. J. *96*, 35–44.

Vargas, E., Yarov-Yarovoy, V., Khalili-Araghi, F., Catterall, W.A., Klein, M.L., Tarek, M., Lindahl, E., Schulten, K., Perozo, E., Bezanilla, F., et al. (2012).

An emerging consensus on voltage-dependent gating from computational modeling and molecular dynamics simulations. J. Gen. Physiol. *140*, 587–594.

Wall-Lacelle, S., Hossain, M.I., Sauve, R., Blunck, R., and Parent, L. (2011). Double mutant cycle analysis identified a critical leucine residue in the IIS4S5 linker for the activation of the Ca(V)2.3 calcium channel. J. Biol. Chem. *286*, 27197–27205.

Wang, C., Bradley, P., and Baker, D. (2007). Protein-protein docking with backbone flexibility. J. Mol. Biol. *373*, 503–519.

Yarov-Yarovoy, V., Baker, D., and Catterall, W.A. (2006a). Voltage sensor conformations in the open and closed states in ROSETTA structural models of K(+) channels. Proc. Natl. Acad. Sci. USA *103*, 7292–7297.

Yarov-Yarovoy, V., Schonbrun, J., and Baker, D. (2006b). Multipass membrane protein structure prediction using Rosetta. Proteins *62*, 1010–1025.

Yarov-Yarovoy, V., Decaen, P.G., Westenbroek, R.E., Pan, C.Y., Scheuer, T., Baker, D., and Catterall, W.A. (2012). Structural basis for gating charge movement in the voltage sensor of a sodium channel. Proc. Natl. Acad. Sci. USA *109*, E93–E102.